Competition sensitive! Draft of 2022.02.03–08:35

Augmenting Lunar Laser Ranging observations with Very Long Baseline Interferometry

Submitted in response to Research Opportunities in Space and Earth Sciences (ROSES) — 2021 Solicitation: NNH21ZDA001N-PDART, program C.4 Planetary Data Archiving, Restoration, and Tools

Contents

1 Executive Summary

We will develop a tool PlaVDA (Planetary VLBI Data Analysis) for processing Level 1 VLBI data product of Lunar lander observations in a form of time series of cross-and auto- spectra and computation of Level 2 data product in a form of differential phase and group delays as well as phase delay rates. Availability of that tool will open a window of opportunity for VLBI observations of artificial radio sources placed on the Moon that will augment Lunar Laser Ranging observations of retroreflectors placed on the Moon by prior Lunar missions. PlaVDA will be validated using prior VLBI observations of Chang'E3 observations in 2015–2016 that are available at the Crustal Dynamics Data Information System (CDDIS) hosted at NASA. Processing Level 1 data belongs to a realm of radioastronomy and requires deep knowledge of VLBI data analysis technique. Users of Level-2 are planetary scientists. This projects aims to build a bridge between radioastronomy and planetary science communities.

2 Introduction

Due to the course of the 20th century geodesy evolved from a utilitarian technique for measuring land plots to a foundation of navigation and an environmental science. At a level of accuracy coarser than 1000 parts per billion (ppb), the Earth surface is static at scales up to several decades. Measurements with accuracy 100 ppb can detect large earthquakes and polar motion. Measurements with accuracy 10 ppb can detect solid tides and plate tectonics on scales of decades. Measurements with accuracy 1 ppb can reveal the presence of liquid core, crustal deformation due air and ocean mass distribution, and constraint parameters of the visco-elastic response of mantle an parameter of the core.

Geodetic observation on the Moon's surface has a similar potential to reveal dynamics of Moon's crust. The absence of air and water on the Moon facilitates interpretation of crust displacements and irregularities in the Moon's rotation. The era of selenodesy started in 1969 with a placement of the retroreflector on the Moon during NASA Apollo-11 mission. At the moment there are 5 retroreflectors on the Moon that forms the fundamental selenodesy network. These retroreflectors are observed from the Earth's using Lunar Laser Ranging (LLR) technique that determines travel time between a ground station and a retroreflector with a sub-centimeter level of accuracy.

These observations were used for improvement of Lunar orbit, for estimation of Lunar rotation parameters called physical librations, and for determination of Lunar crust displacements caused by tides citepr:will15,r:pav20. Analysis of lunar solid tides that reach $\pm$ 9 cm provides information on dissipation at time scales that have not been probed by laboratory experiments and are only starting to be explored for the Earth. LLR first demonstrated that the Moon has a fluid core by detecting the energy dissipated by the flow of the fluid along the core mantle boundary from analysis of irregularities in the Moon rotation.

However, LLR has its own weakness. Observing from the ground an array of 5 retroreflectors on one side of the Moon that is always turned to the Earth makes separations of variables that describe Moon's orbital motion, rotation, and tides is problematic, which results in correlation between estimates. These correlations make interpretation of results difficult and less certain. New retroreflectors that are planned to be installed during future missions would be able to mitigate these problems to some extent, but will not solve them. The root of the problem is that retrore-

flectors see the Earth always at an angle that varies within several degrees while the coverage in a ranee of $\pm 180^{\circ}$ is optimal for variable separation.

Another technique that is sensitive to Moon's orbital motion, rotation, and deformation is very long baseline interferometry (VLBI). A network of ground based radiotelescopes synchronously observe a radio-beacon or a natural extragalactic source such as active galactic nuclei (AGN). The VLBI data acquisition system digitizes voltage of received emission, records them on disk, and puts time stamps from ultra-stable atomic clock stabilized by a Hydrogen maser. The records are shipped to the analysis center and processed. The first stage of the data analysis computes the time series of cross- and auto-correlation functions. Processing cross- and auto-correlation allows to determine delay of the wavefront arrival to station #2 with respect to station #1 with accuracy better than 1 cm. See Figure 1. VLBI observations are equivalent to a differential one-way ranging between the radio beacon B and ground stations G_1 and G_2 that receive signal emitted by B. The power of VLBI technique for application to planetary sciences comes from its ability to process emission from an artificial beacon and from a natural radio source, such as AGN. Processing of such observations allows to determine a displacement of a radio beacon with respect to an AGN. Since AGNs are located at distances of gigaparsecs (1 gigaparsec is equal to $3.1 \cdot 10^{22}$ meter), coordinate system based in AGNs is inertial. Therefore, differential VLBI observations anchor the instantaneous lander position to the inertial space. Selecting an AGN at a small angular distance from the Moon allows to mitigate errors in modeling path delay in the ionosphere and the neutral atmosphere approximately by a factor of the angular distance between an AGN and the beacon expressed in radians. An ability to measure a position of a lander in the direction tangential to the line of sight is very attractive. The LLR technique is sensitive to the distance along the line of sight, i.e. approximately to orthogonal to VLBI.

3 Motivation and problem statement

Although the potential of VLBI observations for planetary science was realized long time ago, the progress is sluggish due to difficulties with data analysis. VLBI technique is commonly used for imaging of continuum spectrum sources such as AGNs, for differential astrometry between two continuum spectrum source or between a continuum source and a narrow-band sources such as a stellar maser, and for geodesy. Methods of data analysis were developed for these cases. These methods are quite different. When a continuum spectrum source is processed, its spectrum of cross-correlation is determined over the entire range of recorded bandwidth. Processing these data allows to determine reliably group delay since the error of group delay determination is reciprocal to the spanned bandwidth. Processing of a narrow-band emission from natural sources follows a different route, but it is based in the assumption that the frequency of the sources after accounting for the Doppler shift due to Earth's rotation and the orbital motion is constant. Processing of observations of Lunar landers cannot be reduced to processing of natural narrow-band sources because its frequency is changed because of both instability of the beacon signal and the contribution of the Doppler frequency shift that depends on beacon a priori positions that are not known with accuracy that would prevent signal decorrelation.

We propose to develop the methodology for processing of combined VLBI observations of Lunar landers and AGNs. Based on that methodology we will develop a tool that processes VLBI observations and produce a) time series of differential phases between a lander and an AGN as well as their rate of change and b) time series of position offsets of the lander with respect to a

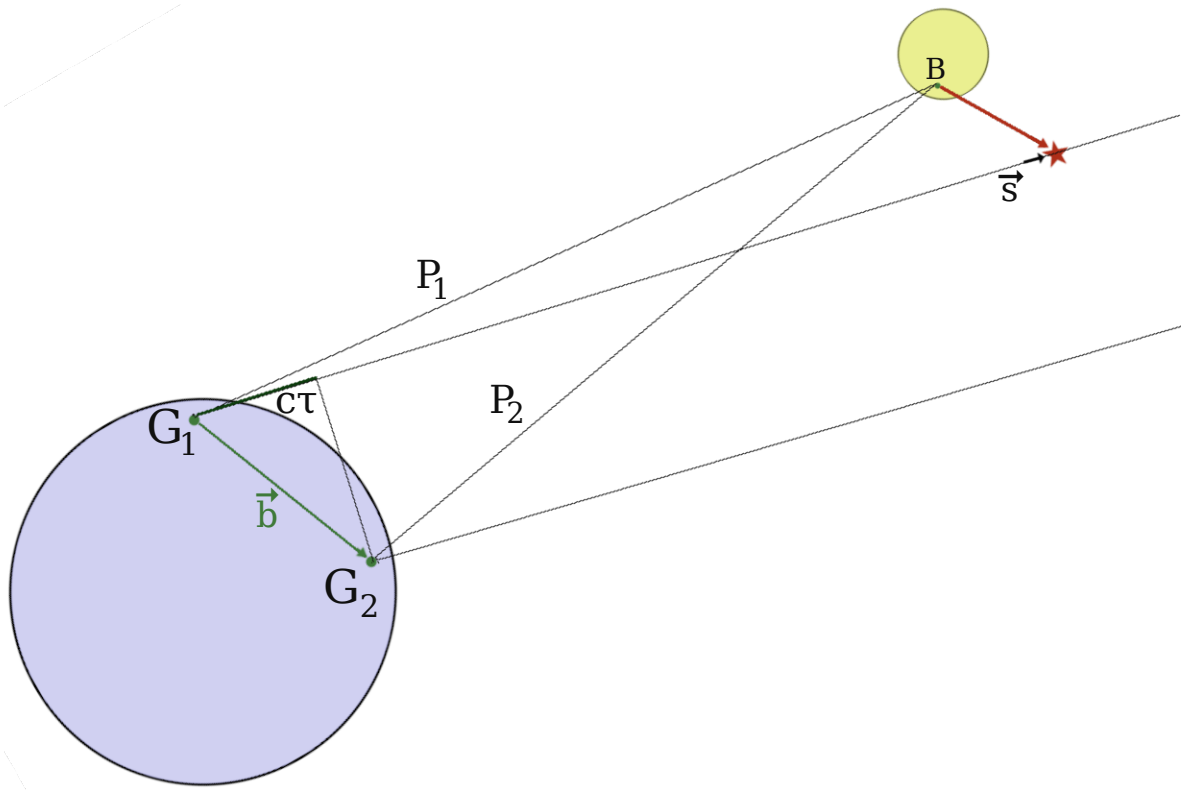

Figure 1: Geometry of VLBI observations. VLBI evaluates path delay $c\tau = |P_1| - |P_2|$ from the satellite and $c\tau = \vec{b} \cdot \vec{s}$ from a background extragalactic radio source. A project of the unit vector of the source position to the celestial is denoted with $\vec{s}$. Baseline vector $\vec{b}$ connects two ground stations G_1 and G_2. Differential observations of both lander B and the extragalactic source S allow to determine precisely vector between B and S.

background AGN. Phase referencing VLBI was successfull used for slow-moving interplaneteray spacecrafts (Fomalont et al., 2010; Duev et al., 2012; Park et al., 2015; Jones et al., 2020), however its use for observations of a Lunar lander that moves fastly over the sky poses an additional challange.

The availability of such a tool will allow the planetary science community to process existing VLBI observations of radio-beacons on the Moon and plan future observations of both dedicated beacons installed for navigation purposes and the signal of opportunity, such as telemetry of spacecrafts operating on the Moon surface. These observations are complimentary to LLR and when analyzed separately, analysis of discrepancies can be used for LLR validation. When analyzed combined, the synergism will be achieved because LLR and differential VLBI observables are orthogonal, which improves variable separation. This leads to improvement in reliability and robustness of results of the combined analysis.

The major motivation of our work is to lift barriers that impede proliferation of VLBI observations of spacecrafts on the Moon.

4 Methodology

VLBI observations of artificial signals from lunar landers can be done in three modes: a) phase tracking, b) geodetic mode using group delays (ΔDOR), and c) phase referencing mode. The phase tracking mode is the easiest. Antennas track the lander. Phase as a function of time is derived from correlation. Informational contents of such measurements is similar to integrated differential Doppler. Such measurements have a questionable value (See f.e., He et al., 2017, for more details). Precision of astrometry observations that use group delays with the wrms of 0.02–0.04 ns is in a range of 1 to 4 nrad depending on the network of ground stations.

Phase-referencing is the main technique in radio astronomy that is de facto a default mode. A scheme of phase-referencing observations is shown in Figure 2. In the simplest case the observing session consists of observing at the beginning and at the end strong amplitude calibrators that are called fringe finders. Observations are made in a sequence C-T-C-T- ... . All antennas of the array dwell on a phase calibrator (C) then slew to target (T), then back, etc. The period of time antennas collect the data is called a scan. Typical scan duration: 15–150 s. The sequence C-T-C-T- is periodically broken and antennas observe for some time atmospheric calibrators. These are call "geodetic blocks". In more sophisticated schemes, more than one phase calibrator is used. The use of more than one calibrator allows to mitigate substantially the impact of residual propagation delay. Such observations are made in a scheme C1-T-C1-C2-T-C2-T-C1- ... or C1-T-C1-C2-T-C2-C3-T-C3-C1- ... . Integration time for calibrators and target are selected depending on source flux density, observing frequency, and the goal of observations. Accuracy of phase referencing depends on target/calibrator separation. A good calibrator within 2° is needed. Quality of results degrades at separations 2–4°, and separations $> 5^\circ$ are avoided (Martí-Vidal et al., 2010). Geodetic blocks last 7–30 minutes and are repeated every 1–5 hours.

Since the Moon is moving with respect to the inertial space with a rate of approximately $30'$ per hour, the angular distance of the beacon with respect to calibrators is changed. Due to Earth rotation the network of observing stations is changed when the Moon is setting at some station and rising at others. Therefore, observations are organized with blocks of 30–50 minutes long. Next block may have different stations and/or different calibrators.

The primary goal of this project is to develop an algorithm that will process phase referencing observations of lunar lander and evaluate offsets of the beacon on a lander with respect to natural extragalactic sources used as calibrators. The data analysis procedure has a number of steps, each step is refining results obtained at the previous step.

4.1 Correlation

Data with records of digitized voltage from receivers are processed with the so-called software correlator, program DiFX (Deller et al., 2007, 2011) supported by the radio astronomy community. This software is adequate for processing data from the calibrators. The only change that is needed is precise computation of path delay from the lander. An extragalactic source is located in the far zone, and path delay is computed assuming the wavefront is parallel. Specifically, expression of Kopeikin and Schäfer (1999) is used. That expression is not applicable for observing object in the near zone. We will develop program sf difx_nz for computation of path delay for the beacon with selenocentric a priori position $\vec{B}$ observed from ground stations G_1 and G_2 at the moment t_1 of the arrival of the wavefront to G_1. Here is the pseudo code:

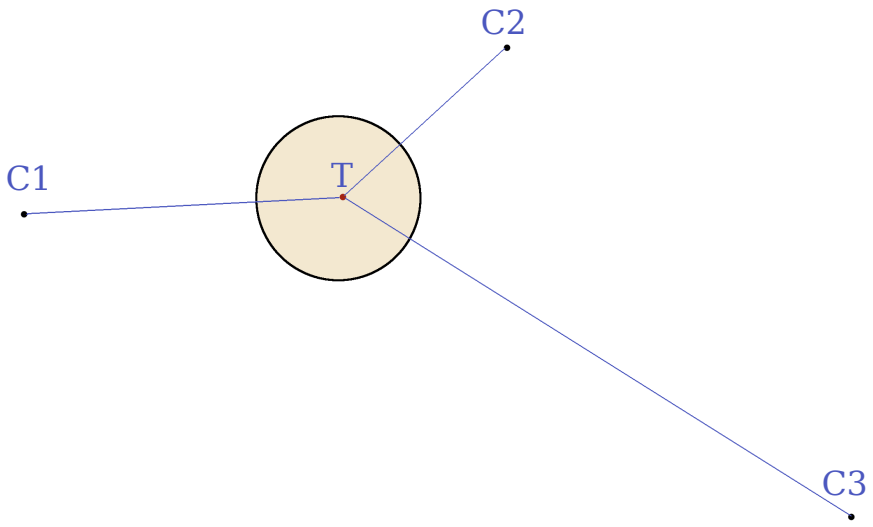

Figure 2: Scheme of nodding observations of spacecraft (T) that transmits narrow-band emission and background AGNs (C1, C2, and C3) that emit in the continuum.

- compute Moon position $\vec{M}$ and velocity $\dot{\vec{M}}$ at t_1 in the celestial inertial coordinate system (CCS)
- compute Moon rotation and Earth rotation matrices $\widehat{\mathcal{R}}_{\oplus}$ and $\widehat{\mathcal{R}}_{m}$ at t_1
- compute position of ground stations and the lander in CSS at t_1
- compute travel time $\tau_1 = |BG_1|(t_1)$ and $\tau_2 = |BG_2|(t_1)$
- compute position of the lander at $t_1 - \tau_1$ and position of G_2 at $t_1 - \tau_1 + \tau_2$
- repeat previous three steps till convergence is reached

This program is based on software package VTD that we previously developed for processing VLBI data of extragalactic sources. We have developed an analytical expression for this procedure as well (Jaron and Nothnagel, 2018).

The correlation is performed with some initial coarse path delay model. We will develop software for preprocessing raw output of the the time series of the cross-correlation spectrum also known as visibilities. This will include correction for the differences $\Delta\tau$ between a precise path delay computed as described above and the one used as a priori during correlation by applying a phase rotation $e^{i2\pi f \Delta\tau(t)}$, where f is the cyclic frequency, splitting the data into observations to lander and the calibrator sources, initial quality control and writing update dataset ready for further analysis.

The principal difficult in processing lander observations is that the lander is moving with respect to inertial system because of Moon's orbital motion and Moons rotation. Applying the a priori Moon's ephemeride and a priori lander positions reduces the residual motion but does not stop it. In order to reach the target accuracy, visibility data should be accumulated and coherently averaged. Coherent averaging requires phase be stable with the averaging interval, i.e. solving for the lander position. This is a non-linear problem, specific for the planetary VLBI observations, and is solved with iterations. The solution we propose is outlined below.

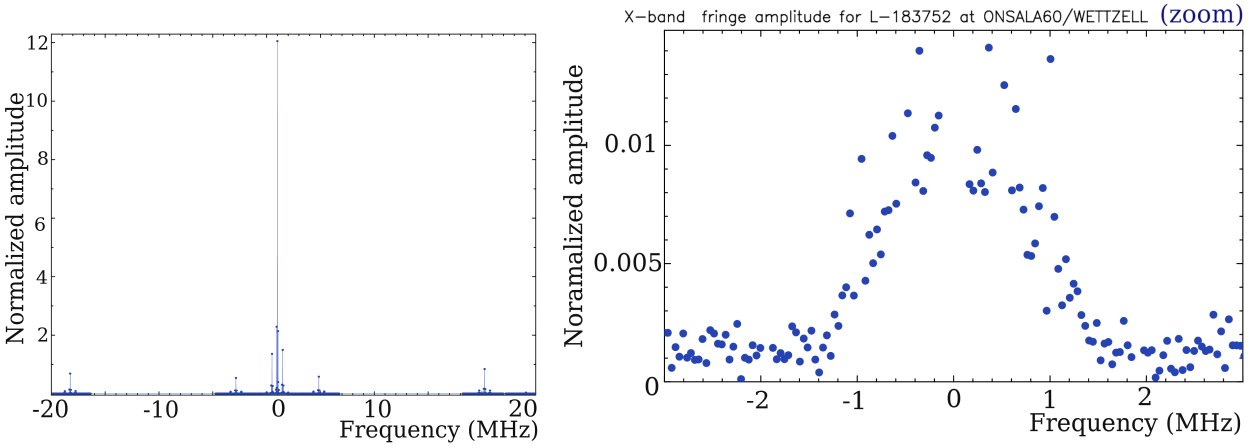

Figure 3: *Left* Amplitude spectrum of the the signal from Chang'E3 lander within 20 MHz bandwidth centered at 8.47 GHz. *Right:* zoom of the spectrum near the signal carrier. This plots does not show a number of narrow-band spectral constituents that are beyond the plotting area.

4.2 Processing group delays

Figure 3 shows spectrum of Chang'E3 lander which is typical. The signal consists of narrow-band carrier, a number of additional narrow-band tones, and the broad-band constituents with a spectrum shape close to the Gaussian function. The width of emitted narrow-band tones range within 0.01–100 Hz depending on the emitter hardware, and the tones are spread over 10–100 MHz. The broad-band signal has width of about 1 MHz and is associated with a telemtery channel. These constituents are processed separately.

First, observations of calibrator sources are processed in a usual way of analysis of continuum spectrum objects. During that stage phase delay τ_p, phase delay rate $\dot{\tau}_p$, and group delay τ_g are adjusted using all the cross-correlation time series of a given scan in such a way that the coherent sum of weighted complex cross-correlation samples c_{kj}

$$C(\tau_p,\tau_g,\dot{\tau}_p) = \sum_k \sum_j c_{kj}\, w_{kj}\, e^{i(\omega_0\tau_p + \omega_0\dot{\tau}_p(t_k - t_0) + (\omega_j - \omega_0)\tau_g)} \qquad (1)$$

reaches the maximum amplitude. Index k runs over time, and index j runs over frequencies. ω_0 and t_0 denote reference circular frequency within the band and the reference time within a scan, ω_j is the subband frequency, and w_{kj} are weights. Then using estimates of group delays and phase delay rates, the visibilities are averaged over time and frequency with the specified averaging intervals, and the averaged visibilities are used for producing images of phase calibrators, i.e. two dimensional distributions of brightness distribution $B(x,y)$.

Second, broad-band group delay from lander observations is computed using a portion of the spectrum with the lander broad-band signal by maximizing $C(\tau_p,\tau_g,\dot{\tau}_p)$ in 1 using the fringe fitting procedure commonly used in VLBI data analysis. Since the bandwidth of the lander board-band spectrum is usually narrower than the recorded bandwidth, the spectrum is multiplied by mask that consists of 0 and 1 to limit the dataset with the data that contains signal from the lander. In a case if the lander spectrum is a priori not known, the procedure for determination of the bandwidth based in analysis of autocorrelation runs. This procedure computes the noise level in the frequency band

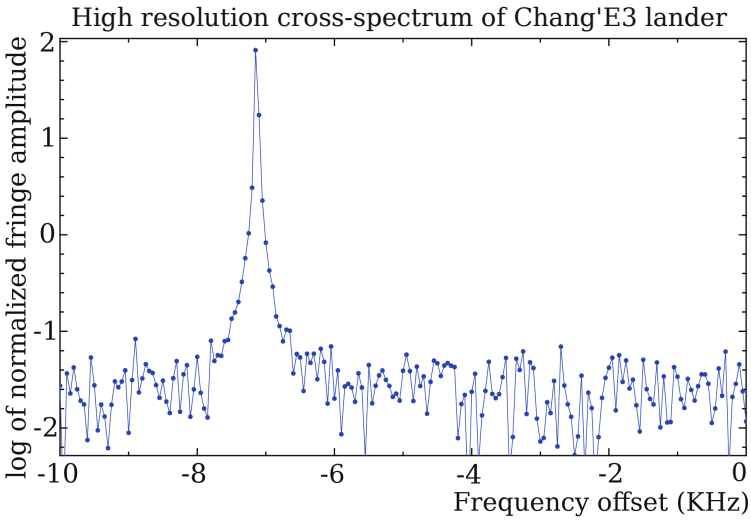

Figure 4: Cross-spectrum of the Chang'E3 carrier with resolution 50 Hz centered at 8.47 GHz.

where it no signal is expected and find the portion of the auto-spectrum that deviates by N times of the root mean square of the noise.

Broad-band group delays from observations of calibrators and the lander are processed in a way similar to processing geodetic VLBI observations. Clock function, atmospheric path delay in zenith direction, and correction to a priori selenocentric lander positions are adjusted in a least square using group delays and least squares. Depending on the design of observations and the spectrum of the emitted signal, position accuracy of the Lunar lander determined that way ranges from 10 to 1000 meters. The adjusted parameters forms the basis for further refinement.

These blocks of the computational procedures are already developed and they are used for processing routine geodetic and astronomical observations. We plan the following work: a) to upgrade existing software for path delay computation to support a lander on a different planet; b) to develop software that calls computational blocks within a pipeline that combines observations of calibrators and the lander; c) to develop a database that would hold results of these computations and intermediate results; d) to develop quality control procedures that would determine outliers in lander observations and flag bad data.

4.3 Processing phase delays and delay rates

Observations of the lander has a narrow band signal from the carrier. Determination of the phase of this signal is the goal of this stage of data analysis.

Frequency of the carrier signal is a function of time. It has a regular constituent due to Doppler shift and a jitter due to the instability of the on board frequency standard. The a priori model used for correlation subtracts the known part of the Doppler shift and retains only small correction due to uncertainty of the lander position. Because of these factors, the spectrum of the carrier broadens (See Figure 4).

We filter out a section of the spectrum that contains the signal from the carrier within $[\omega_o - \omega_b, \omega_o + \omega_b]$ frequency range, where ω_o is the frequency of the maximum. If the model were perfect and the frequency oscillator had no jitter, the interferometer response, i.e. inverse Fourier

transform of the cross-spectrum, would be $\cos(\omega_0 \tau_p)$. We represent the inverse Fourier transform of cross-spectrum $\mathcal{F}^{-1}(C)(t,\omega)$ as

$$\mathcal{F}^{-1}(C)(t,\omega) = A\cos\left(\omega_0 \cdot \left(1+\sum b_i B_i^k(t)\right) \cdot \left(\tau_p + (t-t_0)\dot{\tau}_{pj} + \frac{1}{2}(t-t_0)^2\ddot{\tau}_p\right)\right), \qquad (2)$$

where $B_i^k(x)$ is the basic spline of the kth degree. We will fit b_i, τ_p, $\dot{\tau}_p$, $\ddot{\tau}_p$ using the inverse Fourier transform of time series of the cross-spectra of a given scan within the frequency range $[\omega_o - \omega_b, \omega_o + \omega_b]$. We will use non-linear least squares for using initial values of τ_p and $\dot{\tau}_p$ determined at the previous step. We determine initial values of b_i using the amplitude of visibilities.

We will use unambiguous $\dot{\tau}_p$ and $\ddot{\tau}_p$ collected from all the scans to further refine lander position, and then we will repeat steps of determination of group delay followed by determination of phase delays with updated a priori model of lander positions.

We will develop new software for these steps. That will include search of the frequency range of the carrier $[\omega_o - \omega_b, \omega_o + \omega_b]$, parameter estimation, outlier detection, quality control and bookkeeping.

4.4 Determination of multi-tone group delay

In a case if the lander signal has other narrow-band tones than the carrier, the multi-tone group delay is determined. For instance Chang'E3 has 18 side tone with frequencies -19.75, -19.32, 19.25, 19.19, 18.75, -0.57, -0.50, -0.44, -0.07, 0.06, 0.43, 0.50 0.56, 18.75, 19.18, 19.25, 19.31, 19.75 MHz with respect to the nominal carrier frequency 8470 MHz that can be used for data analysys.

We represent the time series of the cross-spectrum of the side-band tone j at the nominal circular frequency $\omega_0 + \Delta\omega_j$ as

$$C(t,\omega) = A\cos\left((\omega_0+\Delta\omega_j) \cdot \left(1+\sum b_i B_i^k(t)\right) \cdot \left(\tau_p + (t-t_0)\dot{\tau}_p + \frac{1}{2}(t-t_0)^2\ddot{\tau}_p\right)\right). \qquad (3)$$

We process the time series of the side-band tones in a similar way as the main carrier, but we do not estimate coefficients b_i, $\dot{\tau}_p$ and $\ddot{\tau}_p$ keeping them fixed to the values determined from processing the signal carrier. We adjust only correction to $\Delta\omega_j$ and τ_{pj} for each side-band tone using least squares.

The array of phase delays τ_{pj} and their uncertainties determined from the scatter of processed visibilities, as well as the phase delay of the signal carrier are used for evaluation of the multi-tone group delay τ_{mg} and multi-tone phase delay τ_{mp} using weighted least squares with weights set to be reciprocal to phase delay uncertainties:

$$\omega_j \tau_{pj} = \omega_0 \tau_{mp} + (\omega_j - \omega_0)\tau_{mg}. \qquad (4)$$

Since precision of group delay is reciprocal to the spanned bandwidth, precision of multi-band group delay is greater than precision of broad- band group delay. Spanned bandwidth of Chang'E3 broadband signal is $\sim$2 MHz and spanned bandwidth of side-band tones is 39.5 MHz.

We will develop new software to implement these steps of the data analysis pipeline. That will include search for suitable side-band tones, computation of τ_{pj}, evaluation of their uncertainties, outlier detection, quality control, bookkeeping and computation of the multi-band group delay.

4.5 Forming phase delay differences

After the best estimates of phase and group delays from the lander are computed, differential phase and group delays between observations of calibrators and the lander are calculated. First structure phases of calibrated are computed for a given observations using the 2D Fourier transform of the brightness distribution of a calibrators that takes into account deviation of source brightness distribution from a δ-function. Structure phase and group delays of calibrators are subtracted from those computed during fringe fitting. Then time series of phase delays, phase delay rates and group delays of calibrator are expanded into basis spline functions with applying smoothing constraints and group and phase delays of calibrators are interpolated to epochs t0, t1, t2, t3 ... of lander observations.

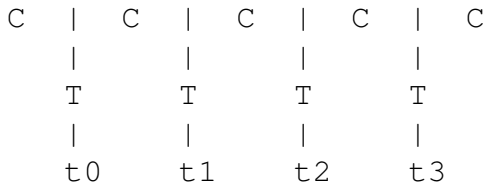

The time series of differential phase and group delays are produced by differencing data from the calibrator and the lander referred to the common epoch and common frequency. These differential phase and group delays form the basis for further analysis.

We will develop new software for interpolation of phase and group delays of calibrators sources and computation of differential phase and group delays. We will incorporate existing imaging software into the data analysis pipeline.

4.6 Differential imaging

Ambiguities in differential phase delay have to be resolved before their use in the geodetic analysis. This is a critical part of the analysis. The feasibility of resolving phase delay ambiguity depends on the signal spectrum, signal strength, and experiment design. A general approach is to use group delay as a starting point with imposing constraint. Differential group delay of a signal from the broad-spectrum constituent of the lander signal (See right plot in Figure 3) of the lander is unambiguous. The multi-tone group delays of the lander have ambiguities that are reciprocal to the minimum frequency difference between tones. Since mutli-tone group delay ambiguity spacings are large (15.6 μs or 4.7 km for Chang'E3), broad-band group delays are precise enough to resolve these ambiguities.

If accuracy of the group delay multi-band delay determination is better than 1/6 of the ambiguity spacing that is reciprocal to the carrier frequency (118 ps or 4 cm for Chang'E3), then ambiguities are resolved easily. In other cases additional information should be used to provide constraints.

At all previous steps cross-correlation from observations at different baselines was processed separately. The ambiguity resolution process commences with a transformation of baseline-based differential phases to station-based phases and then back to baseline-based quantities. The closure condition $\tau_{12} - \tau_{13} + \tau_{23} = 0$ referred to the same time epoch is held for a path delay related to the common epoch at baselines between any three stations. This process eliminates integer ambiguities that would break the closure conditions. Then, the visibility data are gridded, amplitude

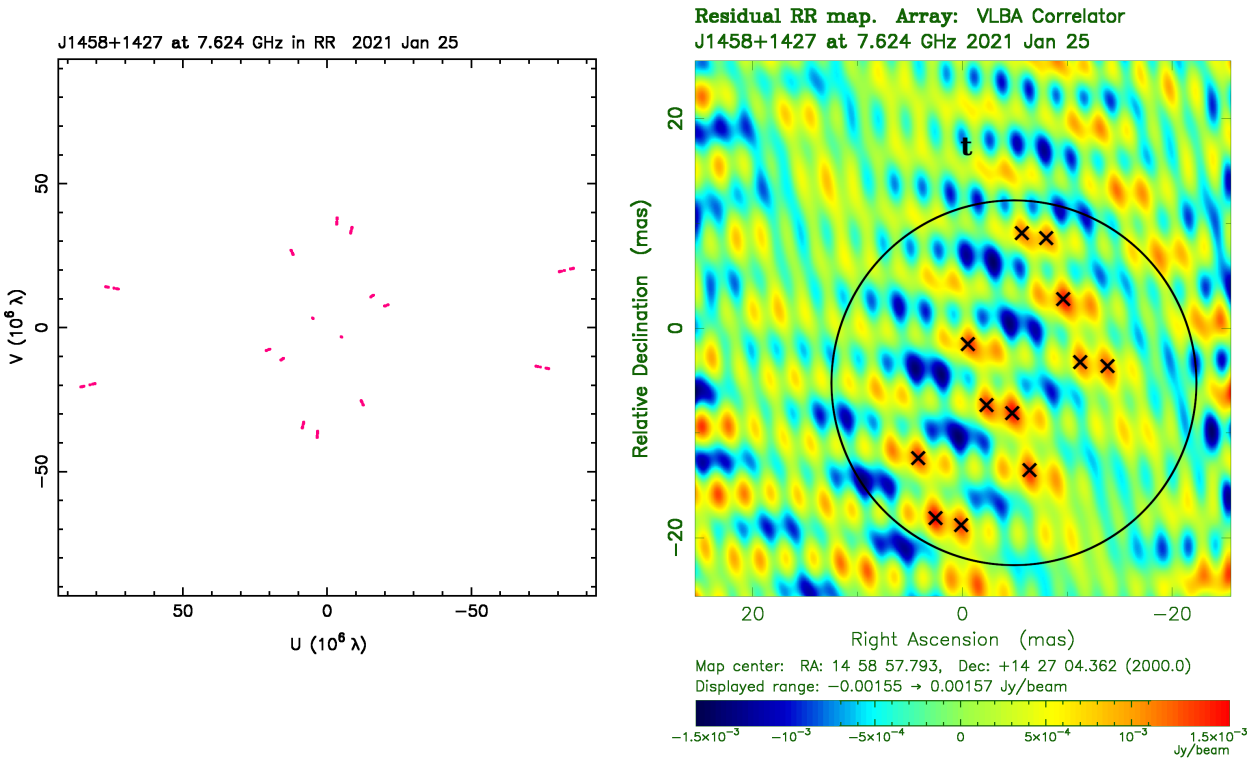

Figure 5: Example of a dirty image. *Right:* Dirty image of J1458-1427 in a snap-short observation at a 5-station VLBA sub-network before phase self-calibration. × sign shows maxima at the image. *Left:* *uv*-coverage of these observations.

is replaced with a constant 1 Jy, and a hybrid imaging process is executed using only the phase self-calibration loop. If the image quality is good, then its maximum provides the offset of lander at the reference epoch with respect to the latest a priori model used. The lander position is fitted to that position offset, the updated model is applied, updated phase delays are computed and the phase delay ambiguity is resolved with respect to the predicted phase. These phase delays are used for the final parameter adjustment and assessment of the position errors.

The true image of the lander is expected to be a δ-function. Phase noise in the image will cause a deviation of the image from the δ-function. The sparseness of observations will cause peaks and negative flux densities. Inaccuracy in a priori lander positions will cause residual motion of the lander with respect to the calibrator, which will result in image smearing. Figure 5 shows dirty image (i.e. before phase and amplitude self-calibration) of J1458+1427 that was observed in one scan at a 5-station VLBA sub-network using 60 second integration time as an illustration of how a raw lander radio-image recovered from VLBI data may look.

This image shows a number of maxima. However, the previous adjustment of the lander position limited the number of maxima to consider. A black circle in Figure 5 shows an error circle from these adjustments for illustrative purposes. Maxima that above some level with respect to the main maximum are shown with sign ×. A coordinate of each point on an image is tied to the position of the calibrator that is taken from the catalogue of absolute positions of AGNs that were determined in numerous programs of absolute astrometry (Beasley et al., 2002; Fomalont et al., 2003; Petrov et al., 2005, 2006; Kovalev et al., 2007; Petrov et al., 2008; Condon et al.,

2017; Petrov and Taylor, 2011; Schinzel et al., 2015, 2017; Fey and Charlot, 1997; Petrov et al., 2011a,b; Petrov, 2011, 2012, 2013; Gordon et al., 2016; Shu et al., 2017; Petrov et al., 2019; Popkov et al., 2020; Petrov, 2021). The algorithm checks all maxima and for each maximum executes the following procedure. First, it determines right ascension and declination of the maxima in the inertial coordinate system from the image. Second, it adjusts lander positions in the selenocentric coordinate system. Third, it computes path delay using adjusted positions for all used observations. Fourth, it forms residuals between computed path delays and observed differential phase and group delays between computed path delay rate and observed path delay rate. Fifth, the algorithm finds a set of N admissible integer ambiguities for each observable at a given baseline and a given scan. Parameter N can be set to a range of 2 to 10 depending on data quality. Sixth, the algorithms computes statistics of residuals. In a case of correctly resolved phase delay ambiguities, the differential phase delay residuals have zero mean and the standard deviation that is consistent with noise in data and residual atmospheric fluctuations. In a case of incorrectly resolved ambiguities, differential phase delay residuals are biased and have an excessive scatter. The algorithm evaluates the probability of false selection of integer ambiguity based on statistics of the residuals and selects those ambiguities that provide the minimum. The algorithm processes all maxima at the image and selects that maxima that provides the minimum of the probability of false phase delay ambiguity among all admissible maxima. As a results of this process, ambiguity-free estimates of phase delay and better estimates of lander positions are computed. Improved positions of the lander are used to re-compute differential phase delays, re-image the lander and repeat the procedure. The iterations are stopped when convergence is reached.

We expect image quality of the lander over 30 or 50 minute integration time will be better than at Figure 5, but we our algorithm is expected to converge to a solution that even in a case of a poor image. Imaging the lander dramatically reduces the number of admissible combinations of integer ambiguities.

We will develop software for implementation of the above algorithm. We will develop software that examines probability of false ambiguity resolution, computes uncertainties of phase and group delays, positions of the lander, and examine convergence.

4.7 Analysis of differential phase delays

The time series of differential phase delays $\Delta\tau_p$, phase delay rates $\Delta\dot{\tau}_p$, and phase delay accelerations $\Delta\ddot{\tau}_p$ are used for a final estimation of lander positions using least squares. Then adjustments of lander positions, phase delay ambiguities, as well as parameters of the signal carrier frequency jitter b_i, are used as a priori for the last round of data analysis of the original visibility data with applied outliers flagging. Inaccuracy in the a priori lander position resulted in a residual motion of the lander. That affected motion caused additional errors that are eliminated in the final round of data analysis.

Analysis of residual visibilities allows to compute errors in phase delays and phase delays rates. The outcome of this analysis are a) improved lander position and estimates of its uncertainty; b) time series of ambiguity free differential phase delays, group delays, phase delay rates and phase delay acceleration, as well as their uncertainties.

We will develop software for computation of the final position of the lander and its position offset with respect to calibrator sources. We will develop software that will generate database files in VGOSDB format adopted by the International VLBI Service for Geodesy

and Astrometry and put there a) time estimates of phase delay, phase delay date, phase acceleration, group delays; b) time series of lander position offsets with respect to calibrator sources; and c) auxiliary information about VLBI observations that is present in VGOSDB databases.

5 Proposed work

We aim to develop a semi-automated tool PlaVDA that would ingest the correlator output of VLBI observations of a lander and extragalactic sources that can be considered as a Level 1 data product and compute observables that are suitable for scientific analysis in depth: time series of differential phase delays, phase delay rates, group delay as well as a by-product updated positions of the lander. These observable can be considered as a Level 2 data product and they become an input for a combined analysis of VLBI and LLR observations for adjustments of parameters of Lunar tides, improvement of the Moon orbit and other quantities using existing tools such as Geodyn and LUNAR. Scientific analysis of Level 2 data is beyond the scope of the proposed work.

We will use existing open source tools of VLBI data analysis, specifically, library VLBI Time Delay (VTD) for computation of VLBI path delay for extragalactic sources, PIMA — a general purpose fringe fitting software, and DifMAP — a general purpose differential VLBI image software and adapt them for solving the problem of producing ambiguity-free differential phase and group delays. That would require the development of algorithms and implementation them in software

- for computation of path delay of an object on the Moon or other body in the Solar System;
- for estimation of position of an object on the Moon or other body in the Solar System using path delay;
- for evaluation of phase delay from a carrier and side-band tones of an object with residual motion such as a Lunar lander;
- for resolving phase delay ambiguity and evaluation of the probability of using a preliminary image of the lander corrupted by artifacts due to its residual motion;
- for quality control of each step that includes detection of outliers, their flagging, estimation of probability of falls detection and false ambiguity resolution.

We will develop the pipeline software that will combine together existing software programs and those that we will develop for processing Lunar lander data in one package PlaVDA. PlaVDA will execute all the steps described above. It will take the initial cross-correlation data and generate the output database file in VGOSDB format with results of analysis. PlaVDA will accept a plain ascii control file in a format `keyword: value` that describes all steps of the data analysis. Although it is desirable to implement a fully automated data analysis procedure, we do not think it is practical at the moment because of scarcity of available VLBI data suitable for validation. Therefore, we adopt a guided semi-automatic data analysis approach. That means that PlaVDA control file in part will be created manually and in part by other programs. A user will have an ability to insert break points in the pipeline, examine results, if necessary, amend the control file and rerun it. By the end of this guided run, the full control file will be created. Then a user will be in a position to run PlaVDA in a totally automatic fashion. That approach will allow to reproduce results.

5.1 Validation

We will be using two experiments from the OCEL campaign (Observing the Chang'E3 Lander with VLBI) run on 2015–2016 for validation of PlaVDA package. These data are publicly available at CDDIS [1]. Huang et al. (2014); Han et al. (2019); Han et al. (2019); Klopotek et al. (2019) performed analysis of group delays and reached position accuracy 3–10 meters. These results demonstrate that the data are high quality. The experiment included block of phase referencing observations. The authors of the cited papers did not make an attempt to work with phase delays and did not provide publicly accessible tools. We will go beyond what Han et al. (2019); Klopotek et al. (2019) have achieved, process phase delays and make the tools and results of our analysis publicly available.

We expect accuracy of phase delay analysis will be higher than 3–10 meters. Statistics of lander positions collected from analysis of 10 observing sessions will allow us to evaluate the scatter of estimates. Statistics of this scatter will allows us to draw an inference about validity of our approach and whether accuracy of phase delays meet expectations.

5.2 Data management

The input Level 1A data that we will be using for validation are archived at the Crustal Dynamics Data Information System (CDDIS) together with VLBI data for space geodesy. The CDDIS provides tools for data ingest and performs backup. The CDDIS mission is to keep the data for the scientific community indefinitely. It provides access to format descriptions. Future VLBI Lunar lander observations will be archived as CDDIS.

The output of processing Level 1A data in a form suitable for planetary data analysis, Level 2 data, will be archived at CDDIS using VGOSDB format used for archiving geodetic data.

Source code developed in the framework of this project will be https://github.com/nasa under Apache License 2.0.

5.3 Prior work

The team has an extensive experience in processing VLBI data for geodetic and astronomical observations. We have developed software VTD, PIMA, pSolve for data analysis of extragalactic sources and process over 6000 geodetic VLBI experiments and 1000 astronomy observations. We have extensive experience in imaging active galactic nuclei from VLBI observations. We ran a preliminary analysis of two experiments of the OCEL campaign an familiarized ourselves with these data.

5.4 Risk mitigation

Resolving phase delay ambiguities always brings a risk of a failure. Feasibility of phase delay resolution depends on a level of unaccounted errors: if there are systematic errors that are a substantial fraction of the ambiguity spacing, for instance to due instrumental errors in VLBI hardware, then ambiguity resolution is not feasible. Our approach with estimation of the probability of false ambiguity resolution is design to detect such a situation and provide a measure of the phase delay

[1] See as an example https://cddis.nasa.gov/archive/vlbi/ivsdata/swin/2015/20151201_rd1510_v001_swin.tar.bz2

scatter. In a case if the phase delay scatter is low, and therefore, phase delay ambiguity resolution is feasible, there is a risk that the initial lander position based on group delay may be biased. Our approach of generation of a lander image and running a the ambiguity resolution procedure using maxima on the image as initial values will mitigate the risk.

5.5 Future observations

Our validation plan is based on publicly available observations and does not depend on other observations. At the same time the National Radio Astronomical Observatory has awarded to our teem observing time with the Very Long Baseline Array for observations of Lunar Node–1 Payload on the Intuitive Machines NOVA-C Lander (LN–1) in 2022. This opportunity to collect new data and analyze them provides us an additional motivation to develop PlaVDA tool.

6 Deliverables and Outcomes

In a course of the project we will

- develop software tool PlaVDA for processing Level 1A VLBI observations of a Lunar lander. The tool will compute group delays, phase delay, and phase delay rates at a range of epochs and generate Level 2 product in VGOSDB format. We will make the source code of that tool publicly available at https://github.com/nasa.
- process two VLBI experiment of observing Chang'E3 lander and submit Level 2 data product at CDDIS.
- validate Level 2 data product using NASA Geodyn software complex.
- prepare NASA Technical Memorandum with a detailed algorithm description.
- submit a paper to a refereed journal that describe PlaVDA and results of Level 2 validation.

7 Management plan and milestones

The chart below shows the schedule for implementing the tasks. The schedule is arranged to give an approximately uniform deployment of effort for the team.

Table 1: Schedule chart

Activity name	PY1 H1	PY1 H2	PY1 H1	PY1 H2
Development of algorithms for processing group delays	•			
Development of algorithms for processing phase delays	•	•		
Processing existing VLBI data and the tool validation		•	•	
Writing papers and reports				•

The Principal Investigator, Leonid Petrov, geophysicist in Geodesy & Geophysics Laboratory at NASA GSFC will manage the project. He will coordinate the efforts of the team. Leonid Petrov will ...

Erwan Mazarico, geophysicist of NASA GSFC, Code 698 will ...

Visnu Viswanathan, will ...

Frank Lemoine, NASA GSFC, Code 61A, will ...

The software developer, TBD, will ...

The collaborator Frederic Jaron will ...

The collaborator Rüdiger Haas, the principal investigator of VLBI OCEL campaign, with consult the team about details of these observations.

8 References

Beasley, A. J., D. Gordon, A. B. Peck, L. Petrov, D. S. MacMillan, E. B. Fomalont, and C. Ma (2002), "The VLBA Calibrator Survey-VCS1." *Astrophys. J. Suppl. Ser.*, 141, 13–21 doi: 10.1086/339806.

Condon, J. J., J. Darling, Y. Y. Kovalev, and L. Petrov (2017), "A Nearly Naked Supermassive Black Hole." *Astrophys. J.*, 834, 184 doi: 10.3847/1538-4357/834/2/184.

Deller, A. T., W. F. Brisken, C. J. Phillips, J. Morgan, W. Alef, R. Cappallo, E. Middelberg, J. Romney, H. Rottmann, S. J. Tingay, and R. Wayth (2011), "DiFX-2: A More Flexible, Efficient, Robust, and Powerful Software Correlator." *Publ. Astron. Soc. Pacific*, 123, 275 doi: 10.1086/658907.

Deller, A. T., S. J. Tingay, M. Bailes, and C. West (2007), "DiFX: A Software Correlator for Very Long Baseline Interferometry Using Multiprocessor Computing Environments." *Publ. Astron. Soc. Pacific*, 119, 318–336 doi: 10.1086/513572.

Duev, D. A., G. Molera Calvés, S. V. Pogrebenko, L. I. Gurvits, G. Cimó, and T. Bocanegra Bahamon (2012), "Spacecraft VLBI and doppler tracking: algorithms and implementation." *Astronomy & Astrophysics*, 541, A43 doi: 10.1051/0004-6361/201218885.

Fey, Alan L. and Patrick Charlot (1997), "VLBA Observations of Radio Reference Frame Sources. II. Astrometric Suitability Based on Observed Structure." *Astrophys. J. Suppl. Ser.*, 111, 95–142 doi: 10.1086/313017.

Fomalont, E., T. Martin-Mur, J. Border, C. Naudet, G. Lanyi, J. Romney, V. Dhawan, and B. Geldzahler (2010), "Spacecraft navigation using the VLBA." In *10th European VLBI Network Symposium and EVN Users Meeting: VLBI and the New Generation of Radio Arrays*, vol. 10, 66.

Fomalont, E. B., L. Petrov, D. S. MacMillan, D. Gordon, and C. Ma (2003), "The Second VLBA Calibrator Survey: VCS2." *Astron. J.*, 126, 2562–2566 doi: 10.1086/378712.

Gordon, D., C. Jacobs, A. Beasley, A. Peck, R. Gaume, P. Charlot, A. Fey, C. Ma, O. Titov, and D. Boboltz (2016), "Second Epoch VLBA Calibrator Survey Observations: VCS-II." *Astron. J.*, 151, 154 doi: 10.3847/0004-6256/151/6/154.

Han, Songtao, Axel Nothnagel, Zhongkai Zhang, Rüdiger Haas, and Qiang Zhang (2019), "Fringe fitting and group delay determination for geodetic VLBI observations of DOR tones." *Advances in Space Research*, 63, 1754–1767 doi: 10.1016/j.asr.2018.11.018.

Han, SongTao, ZhongKai Zhang, Jing Sun, JianFeng Cao, Lue Chen, Lu Weitao, and Li WenXiao (2019), "Lunar Radiometric Measurement Based on Observing China Chang E-3 Lander with VLBI–First Insight." *Advances in Astronomy*, 2019, 7018620 doi: 10.1155/2019/7018620.

He, Qing-bao, Qing-hui Liu, Sheng-qi Chang, and Xin Zheng (2017), "A New Try of Connecting Phase and Solving Phase Delay in VLBI." *Chin. Astron. and Astrophys.*, 41, 614–625 doi: 10.1016/j.chinastron.2017.11.011.

Huang, Yong, Shengqi Chang, Peijia Li, Xiaogong Hu, Guangli Wang, Qinghui Liu, Weimin Zheng, and Min Fan (2014), "Orbit determination of chang'e-3 and positioning of the lander and the rover." *Chinese Science Bulletin*, 59, 3858–3867 doi: 10.1007/s11434-014-0542-9.

Jaron, Frédéric and Axel Nothnagel (2018), "Modeling the VLBI delay for earth satellites." *Journal of Geodesy*, 93, 953–961 doi: 10.1007/s00190-018-1217-0.

Jones, Dayton L., William M. Folkner, Robert A. Jacobson, Christopher S. Jacobs, Jonathan Romney, and Vivek Dhawan (2020), "Very Long Baseline Array Astrometry of Cassini: The Final Epochs and an Improved Orbit of Saturn." *Astron. J.*, 159, 72 doi: 10.3847/1538-3881/ab5f5d.

Klopotek, Grzegorz, Thomas Hobiger, Ruediger Haas, Frederic Jaron, Laura La Porta, Axel Nothnagel, Zhongkai Zhang, Songtao Han, Alexander Neidhardt, and Christian Ploetz (2019), "Position determination of the chan-e3 lander with geodetic vlbi." *Earth, Planets and Space*, 71, 23 doi: 10.1186/s40623-019-1001-2.

Kopeikin, Sergei M. and Gerhard Schäfer (1999), "Lorentz covariant theory of light propagation in gravitational fields of arbitrary-moving bodies." *Physical Review D*, 60 doi: 10.1103/physrevd.60.124002.

Kovalev, Y. Y., L. Petrov, E. B. Fomalont, and D. Gordon (2007), "The Fifth VLBA Calibrator Survey: VCS5." *Astron. J.*, 133, 1236–1242 doi: 10.1086/511157.

Martí-Vidal, I., E. Ros, M. A. Pérez-Torres, J. C. Guirado, S. Jiménez-Monferrer, and J. M. Marcaide (2010), "Coherence loss in phase-referenced VLBI observations." *Astron. & Astrophys.*, 515, A53 doi: 10.1051/0004-6361/201014203.

Park, Ryan S., William M. Folkner, Dayton L. Jones, James S. Border, Alexander S. Konopliv, Tomas J. Martin-Mur, Vivek Dhawan, Ed Fomalont, and Jonathan D. Romney (2015), "Very Long Baseline Array Astrometric Observations of Mars Orbiters." *Astron. J.*, 150, 121 doi: 10.1088/0004-6256/150/4/121.

Petrov, L. (2011), "The Catalog of Positions of Optically Bright Extragalactic Radio Sources OBRS-1." *Astron. J.*, 142, 105 doi: 10.1088/0004-6256/142/4/105.

Petrov, L. (2012), "The EVN Galactic Plane Survey - EGaPS." *Mon. Not. Roy. Astr. Soc.*, 419, 1097–1106 doi: 10.1111/j.1365-2966.2011.19765.x.

Petrov, L. (2013), "The Catalog of Positions of Optically Bright Extragalactic Radio Sources OBRS-2." *Astron. J.*, 146, 5 doi: 10.1088/0004-6256/146/1/5.

Petrov, L., Y. Y. Kovalev, E. B. Fomalont, and D. Gordon (2005), "The Third VLBA Calibrator Survey: VCS3." *Astron. J.*, 129, 1163–1170 doi: 10.1086/426920.

Petrov, L., Y. Y. Kovalev, E. B. Fomalont, and D. Gordon (2006), "The Fourth VLBA Calibrator Survey: VCS4." *Astron. J.*, 131, 1872–1879 doi: 10.1086/499947.

Petrov, L., Y. Y. Kovalev, E. B. Fomalont, and D. Gordon (2008), "The Sixth VLBA Calibrator Survey: VCS6." *Astron. J.*, 136, 580–585 doi: 10.1088/0004-6256/136/2/580.

Petrov, L., Y. Y. Kovalev, E. B. Fomalont, and D. Gordon (2011a), "The Very Long Baseline Array Galactic Plane Survey–VGaPS." *Astron. J.*, 142, 35 doi: 10.1088/0004-6256/142/2/35.

Petrov, L., C. Phillips, A. Bertarini, T. Murphy, and E. M. Sadler (2011b), "The LBA Calibrator Survey of southern compact extragalactic radio sources - LCS1." *Mon. Not. Roy. Astr. Soc.*, 414, 2528–2539 doi: 10.1111/j.1365-2966.2011.18570.x.

Petrov, L. and G. B. Taylor (2011), "Precise Absolute Astrometry from the VLBA Imaging and Polarimetry Survey at 5 GHz." *Astron. J.*, 142, 89 doi: 10.1088/0004-6256/142/3/89.

Petrov, Leonid (2021), "The Wide-field VLBA Calibrator Survey: WFCS." *Astron. J.*, 161, 14 doi: 10.3847/1538-3881/abc4e1.

Petrov, Leonid, Alet de Witt, Elaine M. Sadler, Chris Phillips, and Shinji Horiuchi (2019), "The Second LBA Calibrator Survey of southern compact extragalactic radio sources - LCS2." *Mon. Not. Roy. Astr. Soc.*, 485, 88–101 doi: 10.1093/mnras/stz242.

Popkov, Alexander V., Yuri Y. Kovalev, Leonid Y. Petrov, and Yuri A. Kovalev (2020), "Parsec-scale properties of steep and flat spectrum extragalactic radio sources from a VLBA survey of a complete north polar cap sample." *arXiv e-prints*, arXiv:2008.06803.

Schinzel, F. K., L. Petrov, G. B. Taylor, and P. G. Edwards (2017), "Radio Follow-up on All Unassociated Gamma-Ray Sources from the Third Fermi Large Area Telescope Source Catalog." *Astrophys. J.*, 838, 139 doi: 10.3847/1538-4357/aa6439.

Schinzel, F. K., L. Petrov, G. B. Taylor, E. K. Mahony, P. G. Edwards, and Y. Y. Kovalev (2015), "New Associations of Gamma-Ray Sources from the Fermi Second Source Catalog." *Astrophys. J. Suppl. Ser.*, 217, 4 doi: 10.1088/0067-0049/217/1/4.

Shu, F., L. Petrov, W. Jiang, B. Xia, T. Jiang, Y. Cui, K. Takefuji, J. McCallum, J. Lovell, S.-o. Yi, L. Hao, W. Yang, H. Zhang, Z. Chen, and J. Li (2017), "VLBI Ecliptic Plane Survey: VEPS-1." *Astrophys. J. Suppl. Ser.*, 230, 13 doi: 10.3847/1538-4365/aa71a3.

9 Biographical Sketches

Leonid Petrov (PI)

Present position:

Geophysicist at NASA GSFC in Geodesy & Geophysics Laboratory at NASA GSFC, VLBI Lead Scientist.

Professional experience:

Since 1988 Leonid Petrov has been working in data analysis of space geodesy and remote sensing data, development of data processing algorithms with the highest accuracy, systems and tools aimed to improvement of the terrestrial and celestial reference frames and Earth orientation parameters. He has developed algorithms and implemented them into software for VLBI scheduling, VLBI post-correlation processing based on cross-spectrum, for computation of theoretical VLBI delay, and for geodetic and astrometric VLBI data analysis based on group delays. He has processed all publicly available VLBI observations suitable for astrometry and geodesy.

Leonid Petrov NASA worked at Goddard Earth Sciences Data and Information Services Center for support of the infrastructure for visualization, analyzing, and access of vast amounts of Earth science remote sensing data. During his carrier has has developed over one million line of code for various scientific applications.

Leonid Petrov has been working on development of advanced methods for processing space geodesy, remote sensing data, and numerical models. He has been working on development and maintenance of the pipeline for prepossessing, analysis, and interpretation of VLBI geodetic experiments that was adopted by the International VLBI Service. He also worked on development and maintenance of the International Mass Loading Service, the International Path Delay Service, the Atmospheric Angular Momentum Service, and the Network Earth Rotation Service.

Management experience:

Managed twenty seven projects under various astronomy programs at the National Radio Astronomy Observatory, the European VLBI Network, Australian National Telescope Facility, East Asian VLBI Network, National Astronomical Observatory of Japan, Korea Astronomy and Space Science.

Managed seven projects under NASA Earth Surface and Interior program and one project under NASA Global Navigation Satellite System Remote Sensing Science Team as a principal investigator.

Education:

Ph.D. of Russian Academy of Sciences, 1995, Astronomy
M.S. of Leningrad National University, 1988, Astronomy

Selected publications

1. **Petrov, L.**, "The wide-field VLBA calibrator survey – WFCS", (2021), Astronomical Journal, 161(1), 15 (25pp). doi: 10.3847/1538-3881/abc4e1

2. **Petrov, L.**, (2016), "The International Mass Loading Service", International Association of Geodesy Symposia, Springer, vol 146, 79–83. doi: 10.1007/1345_2015_218

3. **Petrov, L.**, T. Natusch, S. Weston, J. McCallum, S. Ellingsen, S. Gulyaev, (2015). "First scientific VLBI observations using New Zealand 30 meter radio telescope WARK30M", Publications of the Astronomical Society of the Pacific, 127, 516–522

4. **Petrov, L.**, (2015), Modeling of path delay in the neutral atmosphere: a paradigm shift, to appear in the Proceedings of the 12th European VLBI Network Symposium and Users Meeting, 7-10 October 2014 Cagliari, Italy http://arxiv.org/abs/1502.06678

5. P. Sarti, C. Abbondanza, **L. Petrov**, M. Negusini, (2010) "Effect of antenna gravity deformations on VLBI estimates of site positions", Jour. of Geodesy, DOI: 10.1007/s00190-010-0410-6.

6. **Petrov, L.**, D. Gordon, J. Gipson, D. MacMillan, C. Ma, E. Fomalont, R. C. Walker, C. Carabajal, (2009) "Precise geodesy with the Very Long Baseline Array", Journal of Geodesy, vol. 83(9), 859.

7. **Petrov, L.**, (2007) "The empirical Earth rotation model from VLBI observations", Astronomy and Astrophysics, vol. 467, p. 359.

8. **Petrov, L.**, C. Phillips, A. Bertarini, A. Deller, S. Pogrebenko, A. Mujunen, (2009) "The use of the Long Baseline Array in Australia for precise geodesy and absolute astrometry", Publications of the Astronomical Society of Australia, 26(1), 75-84.

9. **Petrov, L.**, J.-P. Boy, (2004) "Study of the atmospheric pressure loading signal in VLBI observations", Journal of Geophysical Research, 10.1029/2003JB002500, vol. 109, No. B03405.

10. **Petrov, L.**, C. Ma, (2003) "Study of harmonic site position variations determined by VLBI", Journal of Geophysical Research, vol. 108, No. B4, 2190.

11. **Petrov, L.**, O. Volvach, N. Nesterov, "Measurements of horizontal motion of the station Simeiz using VLBI", (2001) Kinematic and Physics of Celestial Bodies, Vol. 17, N5, p. 424–436.

There are 59 peer reviewed works with a total of 2347 citations. Hirsch index 26.

10 Summary of Work Effort

g

11 Current and pending support

Current and pending support — Principle Investigator Leonid Petrov

12 Budget Justification (narrative) including facilities and equipment

13 Budget Details (redacted)